http://dx.doi.org/10.5012/bkcs.2014.35.7.2049

Synthesis of Highly Dispersed and Conductive Graphene Sheets by Exfoliation of Preheated Graphite in a Sealed Bath and its Applications to Polyimide Nanocomposites

Muhammad Mohsin Hossain,[†,§] Jae Ryang Hahn,[†,*] and Bon-Cheol Ku[‡,*]

[†]*Department of Chemistry and Bioactive Material Sciences and Research Institute of Physics and Chemistry, Chonbuk National University, Jeonju 561-756, Korea. [*]E-mail: jrhahn@jbnu.ac.kr*
[‡]*Carbon Convergence Materials Research Center, Institute of Advanced Composite Materials, Korea Institute of Science and Technology (KIST), Jeollabuk-do 565-905, Korea. [*]E-mail: cnt@kist.re.kr*
Received January 28, 2014, Accepted March 17, 2014

A simple method for exfoliating pristine graphite to yield mono-, bi-, and multi-layers of graphene sheets as a highly concentrated (5.25 mg/mL) and yielded solution in an organic solvent was developed. Pre-thermal treatment of pristine graphite at 900 °C in a sealed stainless steel bath under high pressures, followed by sonication in 1-methyl-2-pyrrolidinone solvent at elevated temperatures, produced a homogeneous, well-dispersed, and non-oxidized graphene solution with a low defect density. The electrical conductivities of the graphene sheets were very high, up to 848 S/cm. These graphene sheets were used to fabricate graphene-polyimide nanocomposites, which displayed a higher electrical conductivity (1.37 S/m) with an improved tensile strength (95 MPa). The synthesized graphene sheets and nanocomposites were characterized by transmission electron microscopy, scanning electron microscopy, atomic force microscopy, X-ray photo-electron spectroscopy, and Raman spectroscopy.

Key Words : Graphene sheets, Thermal exfoliation, Polyimide nanocomposites, Electrical conductivity, Tensile strength

Introduction

Graphene is formed by a single atomic layer of sp^2-bonded carbon atoms arranged in a honeycomb lattice and exhibits remarkable electronic, thermal, and mechanical properties.[1-3] Several techniques for preparing graphene sheets have been developed since 2004.[4] Chemical vapor deposition[5] and epitaxial growth[6,7] yield graphene with a relatively small number of defects, making these techniques promising for applications in electronic devices; however, these surface-based techniques are not scalable to large scale manufacturing applications. Larger quantities of graphene sheets can be produced *via* physical or chemical exfoliation of graphite.[8,9] These techniques are relatively cheap and versatile as they can be combined with other chemical treatments.

Exfoliation techniques involve separating the stacked parallel layers of graphite. Although the van der Waals attraction forces among sheets are sufficiently weak that the sheets can slide past one another along the direction perpendicular to the *c*-axis, the attraction is strong enough to hinder the complete exfoliation of graphite into individual sheets. Exfoliation techniques can be categorized into three classes: mechanical, thermal, and other exfoliation techniques, including electrochemical methods. Pristine graphite can be exfoliated mechanically and thermally. Direct mechanical exfoliation produces high-quality graphene layers with good crystalline structures, low defect densities, and high conductivities; however, the yields from pristine graphite are usually low.[10,11] For example, the sonication of graphite in an organic solvent normally produces graphene in a yield of less than 1%.[10] Therefore, expanded graphites, such as graphite intercalation compounds (GICs) or graphite oxides, have been used as precursor materials for thermal or mechanical exfoliation. These compounds feature larger interlayer spacing than are present in pristine graphite.[12] This large spacing weaken the van der Waals interactions and facilitate exfoliation. Rapid heating of the intercalated GICs produces expanded graphite that contains partially oxidized graphitic platelets.[13]

Expanded graphites provide better single sheet yields than the direct exfoliation of pristine graphite; however, graphene sheets obtained from these precursors contain many defects or functional groups and, thus, exhibit relatively poor electrical conductivities. Therefore, the production of high-quality graphene with few defects and with a good electrical conductivity requires exfoliation from pristine graphite. Highly dispersed and concentrated graphene solutions with low defect densities are necessary for the production of conducting polymer films. Graphene layers are strongly hydrophobic, and exfoliation in polar solvents, such as water, usually requires the use of surfactants or other aids that act as contaminants in graphene applications.

In this work, we demonstrated an efficient method for mechanically exfoliating pristine graphite. The method was combined with a pre-thermal treatment in a sealed bath under high pressures. Pre-thermal treatment followed by immersion in liquid at a reduced temperature is our new technique for graphite exfoliation, and produced non-oxidized graphene sheets with a low defect density without the use of acids, ionic solvents, or oxidizing agents. The resulting

graphene solution remained well-dispersed at a concentration of 5.25 mg/mL for a period of up to 6 months without the presence of stabilizers. The graphene yield from graphite was high, up to 14%. The electrical conductivities of the graphene films and disks prepared from the exfoliated graphene were relatively high. These graphene sheets could be used to fabricate graphene–polyimide (PI) nanocomposite films that exhibited a very high electrical conductivity and better mechanical properties.

Experimental Methods

Chemicals. Pristine graphite was purchased from Alfa Aesar (graphite flakes, 99.8%, 325 mesh, metal basis). 1-Methyl-2-pyrrolidinone (NMP, 99.5%, anhydrous), 4,4'-oxydianiline (ODA, 97%), and benzene-1,2,4,5-tetracarboxylic dianhydride (pyromellitic dianhydride, PMDA, 97%) were purchased from Sigma Aldrich and were used as received. Acetone (99.5%) was purchased from Daejung Chemicals and Metals, Korea.

Instrumental Analysis. Ultrasonication was performed using a tapered microtip at a 40% amplitude (Sonics Vibra-Cell, CV 334, USA). Pristine graphite was heated in a home-built stainless steel reactor under sustained high pressures and temperatures. The electrical conductivity measurements were collected using a 4-point probe (FPP-RS-8, DasolEng, Korea). Spectroscopic characterization was carried out using UV/VIS/NIR spectrophotometry (V670, JASCO, Japan), Raman spectrometry (HORIBA JOBIN YVON, Lab RAM HR, Laser 514.54, USA), and X-ray photoelectron spectroscopy (XPS, AXIS-NOVA, Kratos, USA). Structural characterizations were carried out using field-emission scanning electron microscopy (FE-SEM, S-4700, Hitachi, Japan), high-resolution transmission electron microscopy (HR-TEM, JEOL, JEM-2010, Japan), atomic force microscopy (AFM, SOLVER P47, NT-MDT), and X-ray diffraction (XRD, Xpert Powder) studies. The mechanical properties were measured using a Universal Testing Machine (UTM 5567A, INSTRON, USA).

Pre-thermal Treatment and Dispersion in Solution. Pristine graphite (15 g) was heated in a sealed stainless steel bath at 900 °C for 5 h (at 44 psi) under a N_2 gas environment, followed by cooling to 250 °C at a speed of 4 °C/min (see the scheme in Figure 1). Once the temperature reached 250 °C, the reactor was removed and placed on a preheated hot plate at 200 °C. The sample was then quickly transferred to a glass bottle containing preheated NMP at 180 °C in a Si oil bath. The sample was stirred at 180-190 °C for 25 min under nitrogen, and then cooled to room temperature. The sample was ultrasonicated again using a tapered tip sonicator for 3 h at an amplitude of 40%. After allowing the solution to settle for 140 h, the top 80% of the solution was collected and allowed to settle for several months. The top 80% of the solution was then filtered and weighed after drying at 300 °C for 2 h to quantify and characterize the dispersed graphene layers.

Fabrication of the Graphene Films and Disks. Graphene films were fabricated using a drop-drying process on a silicon wafer that had been pre-heated at 170 °C. The graphene solution was centrifuged at 15,000 rpm for 3 h using a centrifuge (SUPRA 22 K, Hanil Science, Korea) and then dropped onto the Si wafer a few times until the Si surface was fully covered. After applying a droplet, the droplet was allowed to dry at 270-350 °C for 4 h to characterize the electrical conductivity. Graphene disks were fabricated by CrushIR (Digital Hydraulic press, PIKE Technologies, USA). Graphene samples (50–80 mg) were pressed by applying a force of 14 US tons to prepare disks 205–274 μm thick. The electrical conductivity was measured using a 4-point probe instrument. Four types of graphene disk were prepared at a variety of temperatures and solvents under standard pressures in an effort to improve the electrical conductivities of the resulting devices.

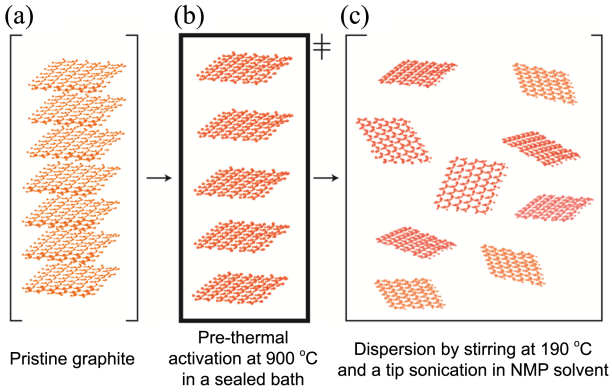

Figure 1. Schematic diagram showing the synthesis of graphene sheets from pristine graphite by suspending thermally activated graphite in NMP as a solvent. (a) Pristine graphite. (b) Thermal activation of graphite layers by heating at 900 °C in a sealed bath for 5 h. (c) The activated graphite temperature was reduced to 25 °C and then suspended in the preheated NMP solvent by stirring at 180–190 °C for 25 min and by sonication using a tapered microtip over 3 h at 40% amplitude.

Fabrication of a Polyimide and a Graphene–Polyimide Nanocomposite Films. ODA (2 g) was added to the glass vial containing NMP solvent (20 mL), followed by stirring for 20 min. The PMDA (2.16 g) was added to the mixture, which was then stirred for 10 min in an ice bath and for 24 h at room temperature to produce polyamic acid (PAA) (Figure 2(a)). The PAA solution was cast onto a clean commercial PI film to prepare a coated film using a bar-coater. The film was then heated at 90 °C in a vacuum for 2 h to prepare an isolated PAA film. The PAA film was separated from the commercial PI film and heated at 350 °C for 4 h to produce a pure PI film (Figure 2(b)). A graphene–PI nanocomposite (1 wt %) was produced by adding ODA (2 g) to a glass vial containing a graphene–NMP solution (7.6 mL, 5.25 mg/mL). NMP solvent (12.4 mL) was added to the glass vial and the solution was stirred for 20 min. PMDA (2.16 g) was added to the solution, and the solution was stirred again for 10 min in an ice bath and 24 h at room temperature. The stirred PAA-graphene nanocomposite solution was then poured onto a clean commercial PI film to prepare a bar cast film. The bar cast film was heated at 90 °C under vacuum

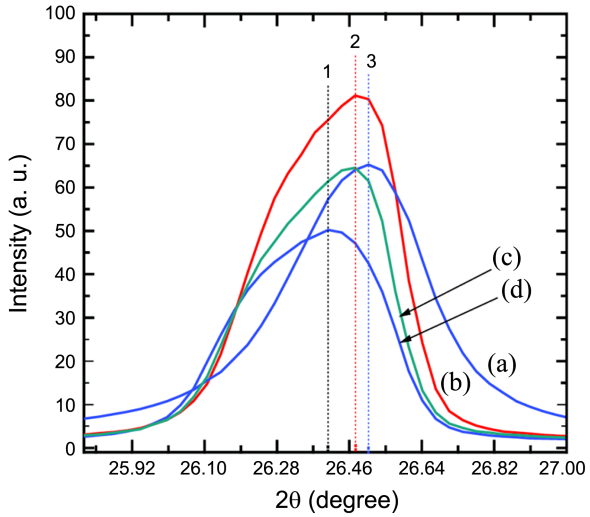

Figure 2. XRD curves obtained from (a) pristine graphite, (b) graphite heated in a sealed bath under nitrogen environment at 900 °C for 5 h, (c) graphite heated at 200 °C for 5 h in preheated NMP, and (d) graphite heated in nitrogen environment at 900 °C for 5 h followed by immersion in preheated NMP solvent at 200 °C for 10 min.

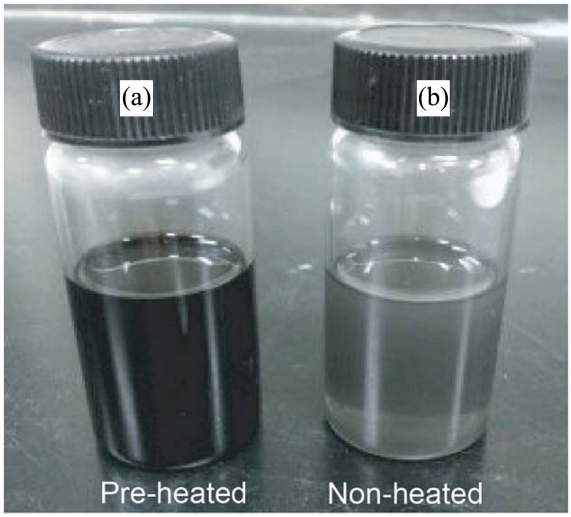

Figure 3. Enhanced dispersion of the graphene sheets. (a) A graphite was pre-heated at 900 °C for 5 h and its temperature was reduced to 200 °C. It was then immersed in NMP solvent by stirring for 25 min with heating at 180–190 °C in NMP. Photograph of this solution was taken after the sample had been permitted to settle for 4 weeks. (b) A graphite sample was stirred for 25 min in NMP at 180–190 °C and allowed to settle for 20 h. The top 80% of the suspension was then collected and is shown in the photograph.

for 2 h and separated from the commercial PI film. The bar cast film was heated in air at 100 °C for 1 h, 200 °C for 1 h, and 300 °C for 1 h in a step-by-step manner using a programmed temperature controller to achieve imidization. The other sample (1 wt %) was prepared by vacuum heating at 90 °C for 2 h followed by heating in air at 350 °C for 4 h. The 5 wt% samples were prepared in a similar manner. Here, a graphene solution (5.25 mg/mL) was centrifuged at 17,000 rpm for 10 h. The bottom 35% portion solution was diluted to a concentration of 10 mg/mL. The graphene solution (20 mL, 10 mg/mL) was used to prepare a 5 wt % polyimide–graphene nanocomposite film in a similar manner (Figure 2(c)). The two 5 wt % samples were heated in vacuum at 90 °C for 2 h. One of them was heated in air at 350 °C for 4 h and the other at 450 °C for 1 h, respectively. All samples were heated at various temperatures to understand the effects of the heating temperature on the electrical conductivity and mechanical properties. Each imidization reaction was carried out in air at 300–450 °C. The PAA film and its composites were converted to its corresponding polyimide film at a high temperature (300–450 °C) by evaporating away the H_2O.

Results and Discussion

Preparation of a Well-Dispersed Graphene Solution. Pre-thermal treatment of the pristine graphite at 900 °C in a sealed stainless steel bath under a nitrogen atmosphere (~44 psi) was presumed to thermally activate the graphite and expand the layers to facilitate exfoliation. During the heating process in a sealed bath, the thermal energy may expand the graphite and build up stress between adjacent graphitic layers. Preheating graphite at elevated temperatures was found to be crucial for the subsequent mechanical ultrasonic exfoliation process. This was confirmed by comparing a graphene dispersion formed from pre-heated or non pre-heated samples (Figure 3). A very dark homogeneous black solution (Figure 3(a)) was obtained from the solution fraction collected from the top 80% of the pre-heated solution after 4 weeks of settling. Only a small amount of precipitant was observed to form over a three months period. On the other hand, the non-pre-heated sample, which was allowed to settle over 20 h, was almost transparent, as shown in Figure 3(b). The expanded or thermally activated pristine graphite was clearly suspended in the NMP solvent. Both the pre-heated and non-pre-heated samples were stirred for 25 min at 180–190 °C to form a dispersed NMP solution. The solutions were then sonicated using a tapered microtip for 3 h to improve the dispersion. An additional set of experiments was conducted to investigate the pressure effects on the efficiency of graphite exfoliation. The graphite solutions were heated to 250–260 °C at 900 or 1500 psi in a Parr reactor under nitrogen. These investigations showed that high pressures were not critical for graphite exfoliation.

In order to determine the crucial factors for the highly efficient exfoliation, we measured XRD spectra from four types of graphite samples (Figure 4). As a reference, XRD spectrum of pristine graphite was taken (curve *a*). Curve *b* is a spectrum measured from a graphite sample heated at 900 °C for 5 h in nitrogen environment followed by cooling to room temperature. Curve *c* shows a spectrum obtained from a sample treated only by heating in NMP at 200 °C without stirring. Graphite was separated by filtration from this solution and dried at 200 °C for 2 h in vacuum. Curve *d* is an XRD spectrum of as-prepared graphite sample which was heated in a sealed bath under nitrogen environment at 900

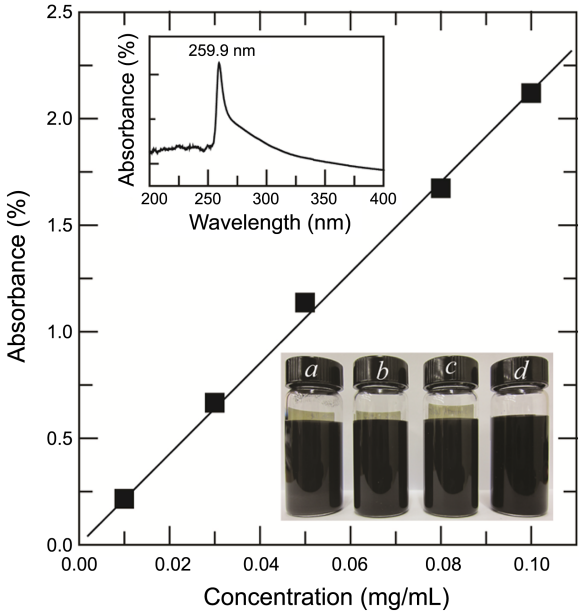

Figure 4. The absorbance of the graphene solution as a function of concentration. Data were fitted using the least-squares method (solid line). The upper inset is an example of UV-visible spectra obtained from graphene solutions. The lower inset is photographs of several graphene sample solutions. (photo-*a*) Graphene solution having a concentration of 5.25 mg/mL. This solution was collected from the top 80% of the sample volume after 140 h sedimentation. (photo-*b*) Another top 80% of the sample volume was permitted to settle for one month. (photo-*c*) Another top 80% of the sample volume was permitted to settle for 5 months. (photo-*d*) Graphene solution centrifuged at 15,000 rpm for 3 h.

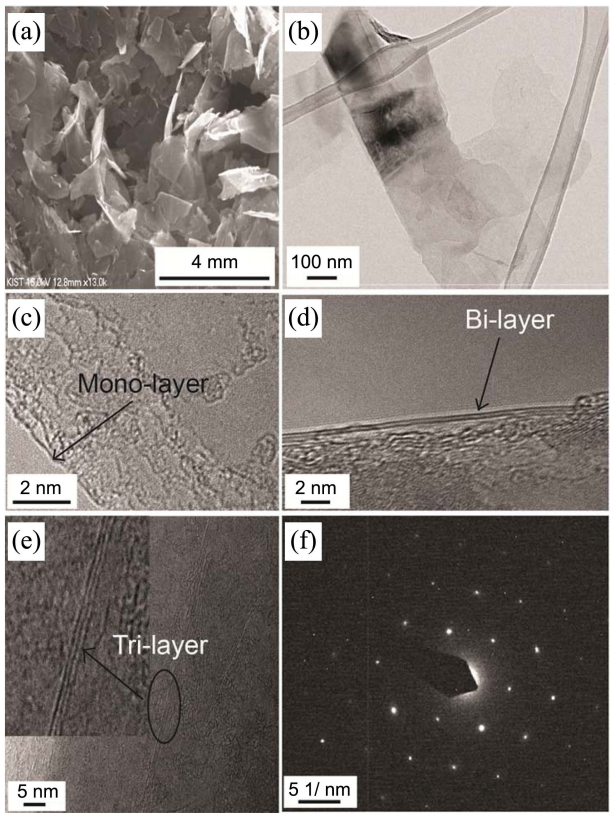

Figure 5. (a) FE-SEM image of graphene layers on a silicon wafer. (b) TEM image of a graphene flake. High-resolution TEM (HR-TEM) images of (c) mono-layer, (d) bi-layer, and (e) tri-layer graphene. (f) Selected area electron diffraction (SAED) patterns obtained from the graphene.

°C for 5 h and then further heated 200 °C in NMP solvent without stirring. The powder sample for XRD was prepared by filtration of graphite solution and drying it at 200 °C for 2 h in vacuum. The dotted lines (1-3 in Figure 4) mark 2 theta values of each XRD spectrum. The lowest value (line 1) from curve *d* indicates the highest spacing between layers. A slight increase in layer-space (line 2) was observed from curves *b* and *c*. Therefore we conclude that the thermal energy should expand the graphite and build up stress between adjacent graphitic layers through the combined heating at 900 °C in a sealed bath and 180-190 °C in NMP solvent.

The dispersion characteristics of the graphene solution in NMP were measured by obtaining the UV/VIS/NIR absorption spectra at various dispersion concentrations (Figure 5). The inset shows the absorption peak at 259.9 nm, which corresponds to a π-π* transition in the C=C bonds of graphene. The absorbance of the graphene solution obeyed the Beer–Lambert law with a coefficient of $\alpha = 2{,}092$ L/g/m. The concentration of a 5.25 mg/mL dispersed graphene solution,

Table 1. Concentration of a dispersed graphene solution and average graphene flake thickness after preparation using a variety of graphite dispersion methods

Concentration (mg/mL)	Synthesis method	Thickness
0.01	Sonication in NMP[10]	Mono-, bi-, and multi-layer
0.02-0.03	Sonication and homogenization ODCB[16]	Mono-, bi-, and multi-layer
0.09-0.25	Dispersion by sodium cholate (centrifuge)[27]	N/A
0.1	Dispersion in water by surfactant[37]	Mono and multi-layer
0.5	Sonication of graphite oxide in water[17]	N/A
0.95	Sonication in ionic liquid[38]	Multi-layer
2	Dispersion in chlorosulfonic acid (centrifuge)[28]	Mono and multi-layer
9.45	Sonication in tetraethylene glycol diacrylate[39]	Multi-layer
5.25	Our work (in NMP)	Mono-, bi-, and multi-layer

ODCB-orthodichloro benzene

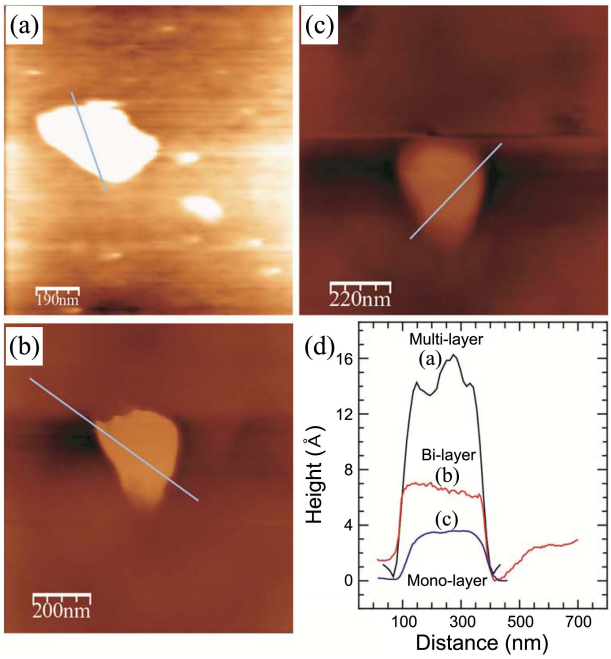

Figure 6. AFM images of (a) multi-layer, (b) bi-layer, and (c) mono-layer graphene sheets adsorbed onto a Si wafer. (d) Cross-sectional cuts along the mono-, bi-, and multi-layered graphene layers.

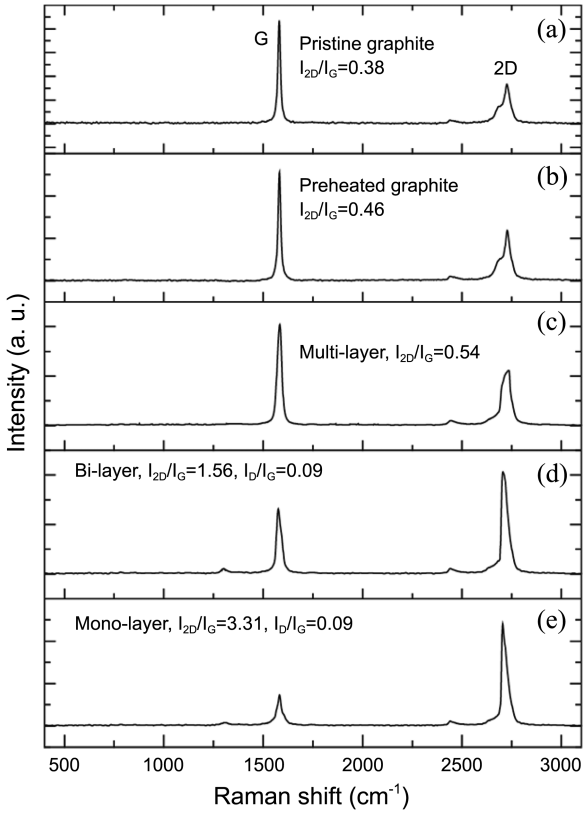

Figure 7. Raman spectra of (curve *a*) pristine graphite, (curve *b*) heated graphite, (curve *c*) multi-, (curve *d*) bi- and (curve *e*) mono-layer graphene. The I2D/IG ratios for the mono- bi- and multi-layer graphene were 3.31, 1.56 and 0.54.

as determined by the Beer–Lambert law, was verified by evaporating 1 mL of the solution at 300 °C over 4 h. After the solvent had been evaporated away, the precipitated graphene was collected and the mass was found to be 5.25 mg. This concentration was very high compared with the dispersion concentrations was reported by others, as listed in Table 1. The dispersed phase was found to be very stable over a period of 6 months. The dispersion stability was tested by collecting the top 80% of the solution (5.25 mg/mL, inset photos in Figure 5) 140 h after preparation. The concentration of this portion of the solution was then measured. The concentration of the top 80% of the solution was found to be 5.25 mg/mL at months 1 (photo *b*) and 5 (photo *c*). The solution was centrifuged at 15,000 rpm for 3 h, and the centrifuged portion (photo *d*) remained very dark for 5 months. Graphene sheets may be precipitated by centrifuging a graphene solution for more than 3 h at 17000 rpm. The graphene yield from the graphite was calculated to be as high as 14%, after three cycles of sonication and collection of the graphene.

Characterization of the Graphene Sheets, Films, and Disks. The shapes of the graphene sheets were characterized by FE-SEM and TEM. A few drops of the graphene solution were deposited onto a silicon wafer and dried. Figure 6(a) shows an FE-SEM image of the dispersed graphene sheets, which consisted of thin nearly flat graphene with little folding. TEM image (Figure 6(b)) indicated that the graphene sheets were less than 1 μm in length. The average thickness and distribution of the graphene sheets were characterized by HR-TEM, and Raman spectroscopy. HR-TEM images confirmed the presence of mono-, bi-, and tri-layer graphene

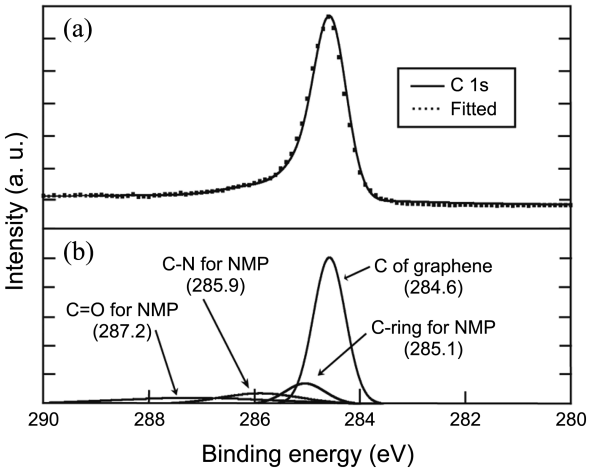

Figure 8. (a) XPS spectrum of the C1s curve (solid line) and fitted curve (dotted line). (b) The deconvoluted curve corresponds to the presence of C=O (287.2), C-N (285.9), and C-ring (285.1) groups, which indicates the presence of NMP solvent impurities.

(Figures 6(c)-6(e)). The inset in Figure 6(f) shows the selected area electron diffraction (SAED) pattern obtained from the graphene film. The hexagonal pattern is characteristic of the graphene structure. AFM images of several sheets (Figure 7(a)-7(c)) also showed the graphene sheets were mono-, bi-, and multi-layer, as revealed by the cross-sectional cuts (Figure 7(d)).

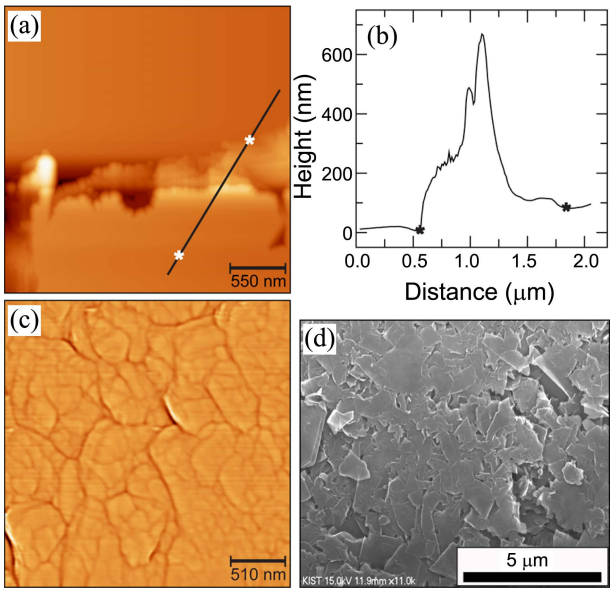

Figure 9. (a) AFM image of a graphene film edge on a Si wafer. (b) A cross-sectional cut along the edge of the graphene film. (c) AFM image of a graphene film surface on a Si wafer. (d) FE-SEM image of a graphene film.

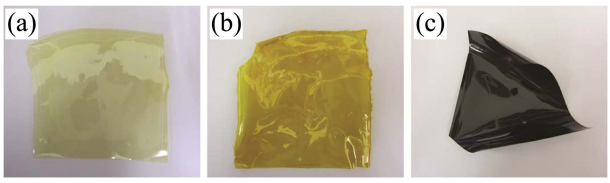

Figure 10. Photographs of (a) a pure PAA film, (b) a pure PI film, and (c) a 5 wt % PI-graphene nanocomposite film.

Table 2. The electrical conductivities of various types of graphene

Conductivity (S/m)	Type
100	Aerogel[20]
1,250	Film[21]
1,500	Film[16]
6,500	Film[10]
7,200	Film[17]
55,000	Film[18]
97,500	Film[19]
84,900	Disk (our work)
72,600	Film (our work)

Raman spectra were collected to determine the average thickness of the graphene sheets. Figure 8 shows the Raman spectra of the graphite and graphene 2D band and the I_{2D}/I_G ratios, which confirmed the presence of mono-, bi-, and multi-layer graphene. The average thickness of the graphene sheets could be assigned based on the 2D band shape.[10] The $I_{2D}/1_G$ ratios of 3.31, 1.56, and 0.54 (curves *e*, *d*, *c*) corresponded to mono-, bi-, and multi-layer graphene sheets.[5,14,15] The intensity of the 2D peak in the mono-layer graphene was higher and the peak shape was sharper than the peaks corresponding to the bi-layer and multi-layer graphene. An example of the optical image is shown in Figure S1a to indicate the location the Raman spectrum (Figure S1b) was obtained. The layer thickness can be determined by Raman spectrum. The relative abundance of mono, bi and multi-layer graphene sheets calculated to be 55%, 25%, and 20%, respectively, which was determined by HR-TEM and AFM analyses in different locations.

The atomic composition of the graphene layers was characterized by XPS (Figure 9(a)), and the percentages of carbon (95.24%) and oxygen (4.76%) were measured. The C1s curve (solid line) from the graphene sample and the curve fit (dotted line) of the XPS spectra (Figure 9(a)) were in agreement over 98% of the curve length. The curves in Figure 9(b) indicated that the graphene sheets contained few impurities corresponding to the C=O, C-N, or C-ring bonds in the NMP. NMP may not have been removed completely[10] from the graphene sheets during the drying process.

Graphene sheets were used to produce graphene films on a Si wafer. Figure 10(a) shows an AFM image of a small area near the edge of the graphene film. Larger-area graphene films are shown in Figures 10(c) (AFM image) and 10(d) (FE-SEM image). The cross-sectional cut (Figure 10(b)) along the edge of the graphene film revealed an average thickness of 83 nm. The electrical conductivity was measured to be 726 S/cm (Table 2). The preparation conditions were optimized by preparing films using different washing solvents and annealing (drying) temperatures. The electrical conductivities of the graphene disks varied with the annealing temperature and the identity of the solvent used during the powder filtration step. The highest electrical conductivity (848 S/cm) was measured in a disk prepared by washing the graphene powder in acetone and annealing at 500 °C for 5 h. Table 2 compares the electrical conductivities of our graphene films and disks with the conductivities obtained from other graphene samples.[10,16-21] The films and disks prepared here yielded high electrical conductivities that are applicable to molecular electronics,[22] transparent electrodes,[23] solar cells,[18,24] field effect transistors,[5,25,26] thin film transistors,[10] conductive polymer composites,[10] transparent conductors,[27] flexible and transparent electronics,[17,28] printed electronics,[19] electrical applications,[29] and micro supercapacitors.[30]

Use of the Graphene Sheets in a Graphene-PI Nanocomposite. Highly conductive and dispersive graphene sheets were used for the preparation of conductive graphene-PI nanocomposites. Pure PI is an insulator (1.7×10^{-15} S/m). Its mechanical properties are summarized in the first row of Table 3. The heating conditions and composite ratio were varied in an effort to improve the electrical conductivities of the nanocomposites (Table 3). The electrical conductivity of the 5 wt % PI-graphene nanocomposite was 1.37 S/m when heated at 90 °C for 2 h under vacuum or at 350 °C for 4 h in air. Table 4 compares the electrical conductivity and mechanical properties of the graphene–polymer nanocomposites prepared here with those obtained using other methods. The nanocomposite prepared here displayed an electrical conduc-

Table 3. Electrical conductivities and mechanical properties of polyimide-graphene nanocomposite films, prepared with a variety of composite ratios and under various heating conditions

Heating condition	Composite ratio (graphene:PI)	Electrical conductivity (S/m)	Tensile strength (MPa)	Young's modulus (GPa)	Tensile strain (%)
A	Pure PI	1.7×10^{-15}	81 ± 5	1.13 ± 0.12	17.8 ± 3.9
B	1:99	0.9×10^{-7}	85 ± 15	1.57 ± 0.28	14.8 ± 2.9
C	1:99	2.35×10^{-7}	90 ± 7	1.40 ± 0.27	20.7 ± 2.95
D	5:95	1.37	95 ± 6	1.55 ± 0.13	18.0 ± 1.8
E	5:95	1.09	66.5 ± 8.5	2.55 ± 0.45	3.76 ± 0.4

The samples A–E are shown in Figures 11(a)–(e), respectively. A) 90 °C (2 h, vacuum) and 350 °C (4 h, air), B) 90 °C (2 h, vacuum), 100 °C (1 h, air), 200 °C (1 h, air), and 300 °C (1 h, air), C) 90 °C (2 h, vacuum) and 350 °C (4 h, air), D) 90 °C (2 h, vacuum) and 350 °C (4 h, air), E) 90 °C (2 h, vacuum) and 450 °C (1 h, air).

Table 4. The electrical conductivities and mechanical properties of various types of graphene-polymer nanocomposites

Matrix in composite	Filler in composite (wt %)	Tensile strength (MPa)	Young's modulus (GPa)	Tensile strain (%)	Electrical conductivity (S/m)
PI[31]	CMG (1)	132	2.78	9.2	2.1×10^{-3}
	GO (1)	121	2.48	10.1	9.8×10^{-4}
PI[32]	FGS (2)	119	1.68	20.1	–
PI[33]	GCA (0.8)	81	1.57	20.5	–
PU[40]	CNT (2)	–	–	–	2.4×10^{-2}
PS[41]	FGS (2.5)[a]	–	–	–	~1
PP[35]	G (1.9)[a]	–	0.98	–	–
PI (our work)	G (5)	95	1.55	18.0	1.37

FGS (functionalized graphene sheet), CMG (chemically modified graphene sheet), GO (graphene oxide), GCA (graphene carboxylic acid), G (graphene). [a]volume%, PI (polyimide), PU (polyurethane), PS (polystyrene), and PP (polypropylene).

tivity that was 15 orders of magnitude than the conductivity of a pure PI film.

The mechanical properties of the films depend on preparation methods. We found the film prepared at 350 °C (for imidization) for 4 h exhibited the better mechanical properties than those obtained from a pure PI film (Table 3). When the film is prepared at 300 °C for imidization, the PAA may not be converted completely to PI. As a result 1 wt % graphene-PI film (condition B in Table 3) showed a lower tensile strength. The tensile strength and tensile strain are measured at the fracture point. At an elevated temperature of 450 °C (condition E), a lower tensile strength was also observed, which may be due to decomposition of nanocomposite film. The lower electrical conductivity (1.09 S/m) with condition E than that of condition D suggest possible decomposition because the conductive path can be disrupted. Therefore we conclude that the heating at 350 °C for 4 h is the optimized condition for the fabrication of graphene-PI film with high mechanical properties and high electrical conductivities. Photograph all of the samples are shown in Figure 11. In general, tensile strain decreases to 99% as the filler content in the polymer matrix increases,[31-35] thereby precluding the use of the nanocomposite in certain high-performance polymer composites. In the present work, the nanocomposite displayed better tensile strength and Young's modulus values compared to the values obtained from a pure PI film having a similar tensile strain values. The good electrical conductivity and mechanical properties of the nanocomposites developed here render the materials useful for a wide range of applications in the aircraft industry,[31] in high-temperature shape memory effect devices,[34] in supercapacitors,[30] and in nanoelectronics.[36]

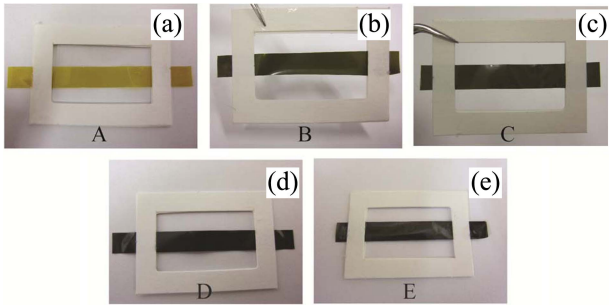

Figure 11. Photographs of the PI and PI-graphene composites. (a) Pure PI film after heating at 90 °C (2 h) in vacuum, then at 350 °C (4 h) in air. (b) A 1 wt % PI-graphene composite film heated at 90 °C (2 h) in vacuum, then at 100 °C (1 h), at 200 °C (1 h), and at 300 °C for (1 h) in air. (c) A 1 wt % PI-graphene composite film heated at 90 °C (2 h) in vacuum, then at 350 °C (4 h) in air. (d) A 5 wt % PI-graphene composite film heated at 90 °C (2 h) in vacuum, then at 350 °C (4 h) in air. (e) A 5 wt % PI-graphene composite film heated at 90 °C (2 h) in vacuum and at 450 °C (1 h) in air.

Conclusions

In conclusion, we developed an efficient and simple method for exfoliating graphite with a high yield of 14%. Pre-

thermal treatment of pristine graphite in a sealed bath under high pressures expanded the graphite layers and enabled the preparation of mono-, bi-, and multi-layer graphene sheets upon sonication in an organic solvent. The graphene solution was highly dispersed in the NMP solvent without the need for surfactants, ionic solvents, or stabilizers. The solution maintained a high concentration of 5.25 mg/mL and was stable for a period of 6 months. The graphene sheets did not undergo oxidation, and the defect density was low. The well-dispersed, stable, and highly concentrated graphene sheets permitted the fabrication of graphene-PI nanocomposite films that exhibited enhanced electrical conductivities, up to 1.37 S/m, and good mechanical properties (a 95 MPa tensile strength) relative to the properties of pure PI.

Acknowledgments. This work was supported by grants from the Korea Institute of Science and Technology (KIST) Institutional program and the Korean government (NRF, MSIP) (2010-0024254 and 2007-0056095). MMH was supported BK21 PLUS program. Financial support from the fundamental R&D program for Core Technology of Materials funded by the Ministry of Trade, Industry & Energy, Republic of Korea, is also acknowledged.

References

1. Lee, C.; Wei, X.; Kysar, J. W.; Hone, J. *Science* **2008**, *321*, 385.
2. Peigney, A.; Laurent, C.; Flahaut, E.; Bacsa, R. R.; Rousset, A. *Carbon* **2001**, *39*, 507.
3. Balandin, A. A.; Ghosh, S.; Bao, W.; Calizo, I.; Teweldebrhan, D.; Miao, F.; Lau, C. N. *Nano Lett*. **2008**, *8*, 902.
4. Novoselov, K. S.; Geim, A. K.; Morozov, S. V.; Jiang, D.; Zhang, Y.; Dubonos, S. V.; Grigorieva, I. V.; Firsov, A. A. *Science* **2004**, *306*, 666.
5. Li, X.; Cai, W.; An, J.; Kim, S.; Nah, J.; Yang, D.; Piner, R.; Velamakanni, A.; Jung, I.; Tutuc, E.; Banergee, S. K.; Colombo, L.; Ruoff, R. S. *Science* **2009**, *324*, 1312.
6. Berger, C.; Song, Z.; Li, T.; Li, X.; Ogbazghi, A. Y.; Feng, R.; Dai, Z.; Marchenkov, A. N.; Conrad, E. H.; Phillip, N. *J. Phys. Chem. B* **2004**, *108*, 19912.
7. Rollings, E.; Gweon, G. H.; Zhou, S. Y.; Mun, B. S.; McChesney, J. L.; Hussain, B. S.; Fedorov, A. V.; First, P. N.; Heer, W. A. D.; Lanzara, A. *J. Phys. Chem. Solids* **2006**, *67*, 2172.
8. Schniepp, H. C.; Li, J. L.; McAllister, M. J.; Sai, H.; Herrera-Alonso, M.; Adamson, D. H.; Prud'homme, R. K.; Car, R.; Saville, D. A.; Aksay, I. A. *J. Phys. Chem. B* **2006**, *110*, 8535.
9. Stankovich, S.; Piner, R. D.; Chen, X.; Wu, N.; Nguyen, S. B. T.; Ruoff, R. S. *J. Mater. Chem.* **2006**, *16*, 155.
10. Hernandez, Y.; Nicolosi, V.; Lotya, M.; Blighe, F. M.; Sun, Z. Y.; De, S.; McGovern, I. T.; Holland, B.; Byrne, M.; Gun'ko, Y. K.; Boland, J. J.; Niraj, P.; Duesberg, G.; Krishnamurthy, S.; Goodhue, R.; Hutchison, J.; Scardaci, V.; Ferrari, A. C.; Coleman, J. N. *Nat. Nanotechnol*. **2008**, *3*, 563.
11. Bourlinos, A. B.; Georgakilas, V.; Zboril, R.; Steriotis, T. A.; Stubos, A. K. *Small* **2009**, *5*, 1841.
12. Dresselhaus, M. S.; Dresselhaus, G. *Adv. Phys*. **1981**, *30*, 139.
13. Chen, G.; Wu, D.; Weng, W.; Wu, C. *Carbon* **2003**, *41*, 619.
14. Reina, A.; Jia, Z.; Ho, J.; Nezich, D.; Son, H.; Bulovic, V.; Dresselhaus, M. S.; Kong, J. *Nano Lett*. **2009**, *9*, 30.
15. Ruan, G.; Sun, Z.; Peng, Z.; Tour, J. M. *ACS Nano* **2011**, *5*, 7601.
16. Hamilton, C. E.; Lomeda, J. R.; Sun, Z.; Tour, J. M.; Barron, A. R. *Nano Lett.* **2009**, *9*, 3460.
17. Li, D.; Muller, M. B.; Gilje, S.; Kaner, R. B.; Wallace, G. G. *Nat. Nanotechnol.* **2008**, *3*, 101.
18. Wang, X.; Zhi, L.; Mullen, K. *Nano Lett*. **2008**, *8*, 323.
19. Jeong, S. Y.; Kim, S. H.; Han, J. T.; Jeong, H. J.; Jeong, S. Y.; Lee, G. W. *Adv. Funct. Mater*. **2012**, *22*, 3307.
20. Worsley, M. A.; Pauzauskie, P. J.; Olson, T. Y.; Biener, J.; Satcher, J. H., Jr.; Baumann, T. F. *J. Am. Chem. Soc*. **2010**, *132*, 14067.
21. Si, Y.; Samulski, E. T. *Nano Lett*. **2008**, *8*, 1679.
22. Berger, C.; Song, Z.; Li, X.; Wu, X.; Brown, N.; Naud, C.; Mayou, D.; Li, T.; Hass, J.; Marchenkov, A. N.; Conrad, E. H.; First, P. H.; Heer, W. A. D. *Science* **2006**, *312*, 1191.
23. Kim, K. S.; Zhao, Y.; Jang, H.; Lee, S. Y.; Kim, J. M.; Kim, K. S.; Ahn, J. H.; Kim, P.; Choi, J. Y.; Hong, B. H. *Nature* **2009**, *457*, 706.
24. Li, X.; Zhang, G.; Bai, X.; Sun, X.; Wang, X.; Wang, E.; Dai, H. J. *Nat. Nanotechnol.* **2008**, *3*, 538.
25. Li, X. L.; Wang, X. R.; Zhang, L.; Lee, S. W.; Dai, H. J. *Science* **2008**, *319*, 1229.
26. Novoselov, K. S.; Geim, A. K.; Morozov, S. V.; Jiang, D.; Zhang, Y.; Dubonos, S. V.; Grigorieva, I. V.; Firsov, A. A. *Science* **2004**, *306*, 666.
27. Green, A. A.; Hersam, M. C. *Nano Lett.* **2009**, *9*, 4031.
28. Behabtu, N.; Lomeda, J. R.; Green, M. J.; Higginbotham, A. L.; Sinitskii, A.; Kosynkin, D. V.; Tsentalovich, D.; Parra-Vasquez, A. N. G.; Schmidt, J.; Kesselman, E.; Cohen, Y.; Talmon, Y.; Tour, J. M.; Pasquali, M. *Nat. Nanotechnol.* **2010**, *5*, 406.
29. Chung, D. D. L. *J. Mater. Sci*. **2004**, *39*, 2645.
30. Gao, W.; Singh, N.; Song, L.; Liu, Z.; Reddy, A. L. M.; Ci, L.; Vajtai, R.; Zhang, Q.; Wei, B.; Ajayan, P. M. *Nat. Nanotechnol*. **2011**, *6*, 496.
31. Huang, T.; Lu, R.; Su, C.; Wang, H.; Guo, Z.; Liu, P.; Huang, Z.; Chen, H.; Li, T. *ACS Appl. Mater. Interfaces* **2012**, *4*, 2699.
32. Chen, D.; Zhu, H.; Liu, T. *ACS Appl. Mater. Interfaces* **2010**, *2*, 3702.
33. Kim, G. Y.; Choi, M. C.; Lee, D.; Ha, C. S. *Macromol. Mater. Eng*. **2012**, *297*, 303.
34. Yoonessi, M.; Shi, Y.; Scheiman, D. A.; Lebron-Colon, M.; Tigelaar, D. M.; Weiss, R. A.; Meador, M. A. *ACS Nano* **2012**, *6*, 7644.
35. Stuerer, P.; Wissert, R.; Thomann, R.; Muelhaupt, R. *Macromol. Rapid Commun*. **2009**, *30*, 316.
36. Wang, S.; Ang, P. K.; Wang, Z.; Tang, A. L. L.; Thong, J. T. L.; Loh, K. P. *Nano Lett*. **2010**, *10*, 92.
37. Lotya, M.; Hernandez, Y.; King, P. J.; Smith, R. J.; Nicolosi, V.; Karlsson, L. S.; Blighe, F. M.; De, S.; Wang, W.; McGovern, I. T.; Duesberg, G. S.; Coleman, J. N. *J. Am. Chem. Soc*. **2009**, *131*, 3611.
38. Wang, X.; Fulvio, P. F.; Baker, G. A.; Veith, G. M.; Unocic, R. R.; Mahurin, S. M.; Chi, M.; Dai, S. *Chem. Commun*. **2010**, 4487.
39. Alzari, V.; Nuvoli, D.; Sanna, R.; Scognamillo, S.; Piccinini, M.; Kenny, J. M.; Malucelli, G.; Mariani, A. *J. Mater. Chem.* **2011**, *21*, 16544.
40. Xu, X. B.; Li, Z. M.; Shi, L.; Bian, X. C.; Xiang, Z. D. *Small* **2007**, *3*, 408.
41. Stankovich, S.; Dikin, D. A.; Dommett, G. H. B.; Kohlhaas, K. M.; Zimney, E. J.; Stach, E. A.; Piner, R. D.; Nguyen, S. T.; Ruoff, R. S. *Nature* **2006**, *442*, 282.